J|A|C|S
ARTICLES
Published on Web 02/26/2002

# Determination of Cα Chemical Shift Tensor Orientation in Peptides by Dipolar-Modulated Chemical Shift Recoupling NMR Spectroscopy

Xiaolan Yao and Mei Hong*

*Contribution from the Department of Chemistry, Iowa State University, Ames, Iowa 50011*

Received September 21, 2001

***Abstract:*** We present a new method for determining the orientation of chemical shift tensors in polycrystalline solids with site resolution and demonstrate its application to the determination of the Cα chemical shift tensor orientation in a model peptide with $\beta$-sheet torsion angles. The tensor orientation is obtained under magic angle spinning by modulating a recoupled chemical shift anisotropy (CSA) pattern with various dipolar couplings. These dipolar-modulated chemical shift patterns constitute the indirect dimension of a 2D spectrum and are resolved according to the isotropic chemical shifts of different sites in the direct dimension. These dipolar-modulated CSA spectra are equivalent to the projection of a 2D static separated-local-field spectrum onto its chemical shift dimension, except that its dipolar dimension is multiplied with a modulation function. Both $^{13}$C−$^{1}$H and $^{13}$C−$^{15}$N dipolar couplings can modulate the CSA spectra of the Cα site in an amino acid and yield the relative orientations of the chemical shift principal axes to the C−H and C−N bonds. We demonstrate the C−H and C−N modulated CSA experiments on methylmalonic acid and *N*-tBoc-glycine, respectively. The MAS results agree well with the results of the 2D separated-local-field spectra, thus confirming the validity of this MAS dipolar-modulation approach. Using this technique, we measured the Val Cα tensor orientation in *N*-acetylvaline, which has $\beta$-sheet torsion angles. The $\sigma_{11}$ axis is oriented at 158° (or 22°) from the C−H bond, while the $\sigma_{22}$ axis is tilted by 144° (or 36°) from the C−N bond. Both the orientations and the magnitude of this chemical shift tensor are in excellent agreement with quantum chemical calculations.

## Introduction

Chemical shift tensors are important parameters of nuclear spins and have been widely used to obtain information on the conformation, dynamics, and orientation of molecules. For example, the isotropic chemical shifts of $^{13}$Cα, $^{13}$C$\beta$, $^{1}$Hα, and $^{1}$H$\beta$ in proteins depend on the secondary structure in a characteristic way.[1−3] Similarly, a conformation dependence of anisotropic chemical shifts has also been observed experimentally[4] and calculated quantum chemically.[5−7] In particular, the Cα chemical shift anisotropy (CSA) is much smaller in α-helical residues than in $\beta$-sheet residues. This structural dependence of CSA has begun to be exploited for conformational studies of proteins in the solid state, where no isotropic molecular tumbling is present to average the anisotropic chemical shift interaction.[8] While much attention has been devoted to establishing correlations between the *magnitude* of chemical shift tensors and the three-dimensional structure of proteins, less is known about the *orientation* of chemical shift tensors and their dependence on protein structure. The best studied chemical shift tensor orientations are those of the amide $^{15}$N and the carbonyl $^{13}$C, which are predominantly influenced by the peptide plane geometry.[9−12] The $^{15}$N chemical shift tensor has the most deshielded (downfield) principal axis roughly parallel to the N−H bond in the peptide plane,[13] while the intermediate principal axis ($\sigma_{22}$) is perpendicular to the peptide plane. For the carbonyl $^{13}$C chemical shift tensor, the most shielded (upfield) principal axis is perpendicular to the peptide plane, while the $\sigma_{22}$ axis is nearly parallel to the CO bond. Not surprisingly, the $^{13}$CO and $^{15}$N chemical shift tensors are affected by hydrogen bonding as well as by local torsion angles, which make them ambiguous probes of protein backbone conformation.[11,14] In comparison, the Cα chemical shift tensor derives its strongest influence from the torsion angles $\phi$ and $\psi$ in each

* Corresponding author: (tel) 515-294-3521; (fax) 515-294-0105; (e-mail) mhong@iastate.edu.

(1) Wishart, D. S.; Bigam, C. G.; Holm, A.; Hodges, R. S.; Sykes, B. D. *J. Biomol. NMR* **1995**, *5*, 67−81.
(2) Spera, S.; Bax, A. *J. Am. Chem. Soc.* **1991**, *113*, 5490−5492.
(3) Iwadate, M.; Asakura, T.; Williamson, M. P. *J. Biomol. NMR* **1999**, *13*, 199−211.
(4) Tjandra, N.; Bax, A. *J. Am. Chem. Soc.* **1997**, *119*, 9576−9577.
(5) Havlin, R. H.; Le, H.; Laws, D. D.; deDios, A. C.; Oldfield, E. *J. Am. Chem. Soc.* **1997**, *119*, 11951−11958.
(6) Asakawa, N.; Kurosu, H.; Ando, I.; Shoji, A.; Ozaki, T. *J. Mol. Struct.* **1994**, *317*, 119−129.
(7) Case, D. A. *Curr. Opin. Struct. Biol.* **1998**, *8*, 624−630.
(8) Hong, M. *J. Am. Chem. Soc.* **2000**, *122*, 3762−3770.
(9) Hartzell, C. J.; Whitfeld, M.; Oas, T. G.; Drobny, G. P. *J. Am. Chem. Soc.* **1987**, *109*, 5966−5969.
(10) Oas, T. G.; Hartzell, C. J.; Dahlquist, F. W.; Drobny, G. P. *J. Am. Chem. Soc.* **1987**, *109*, 5962−5966.
(11) Wei, Y.; Lee, D.; Ramamoorthy, A. *J. Am. Chem. Soc.* **2001**, *123*, 6118−6126.
(12) Lee, D.-K.; Ramamoorthy, A. *J. Magn. Reson.* **1998**, *133*, 204−206.
(13) Harbison, G. S.; Jelinski, L. W.; Stark, R. E.; Torchia, D. A.; Herzfeld, J.; Griffin, R. G. *J. Magn. Reson.* **1984**, *60*, 79−82.
(14) deDios, A. C.; Oldfield, E. *J. Am. Chem. Soc.* **1994**, *116*, 11485−11488.



**10.1021/ja017137p CCC: $22.00** 

residue, since it has no obvious local symmetry or other strong interactions governing shielding.[15] Quantum chemical calculations have shown that, analogous to the chemical shift magnitude difference between helix and sheet, the orientation of the Cα tensor also varies significantly among different conformations. For example, the most deshielded tensor element, $\sigma_{11}$, is oriented on average at ~8° from the C−H bond in sheet residues but changes to ~82° in helical residues. Similarly, the orientation of the $\sigma_{22}$ axis relative to the C−N bond centers at ~60° in helical residues but ~150° in sheet residues.[5]

This large conformational variation of the Cα chemical shift tensor orientation, if verified, could be useful for studying the orientation of membrane peptides and proteins in the solid state. It is also relevant to solution NMR relaxation measurements, which typically assume the Cα chemical shift tensor to be uniaxial along the C−H bond.[4] To date, few experimental measurements of the Cα chemical shift tensor orientation are available.[16,17] The traditional solid-state NMR methods for determining tensor orientations are not practical for various reasons. For example, single crystals are difficult to grow, and static 2D separated-local-field (SLF) experiments[18,19] on polycrystalline samples require $^{13}$Cα and $^{15}$N double labeling, which is not available for most amino acids. The scarcity of $^{13}$Cα and $^{15}$N dual labeling also renders the 1D static dipolar-modulated CSA technique not applicable.[9] On the other hand, techniques based on magic angle spinning (MAS), which restore site resolution without labeling, also have serious limitations. For example, the 2D sideband approach requires inconveniently low spinning speeds.[20] A recent dipolar and chemical shift recoupling technique[21] that reintroduces 2D SLF powder patterns under MAS not only has complex sequence elements but also has inherently low sensitivity, since the experiment requires a third dimension to obtain site resolution.

In this paper, we introduce a 2D MAS dipolar-modulated CSA technique for measuring chemical shift tensor orientations with site resolution, high angular precision, and high sensitivity. We apply the technique to the measurement of the Val Cα tensor orientation in a model compound with $\beta$-sheet torsion angles. These provide benchmark values of the orientation and magnitude of the Cα chemical shift tensor in a structured amino acid, and may facilitate future use of this spin property in structural studies of proteins.

## Materials and Methods

**Materials.** The $^{13}$C-natural abundance methylmalonic acid was purchased from Sigma, and $^{15}N$-tBoc-$^{13}$Cα-glycine was purchased from Cambridge Isotope Laboratories (Andover, MA). Both samples were used without further purification. $^{15}N$-acetylvaline (NAV) was synthesized as described previously[22] and recrystallized by slow evaporation of a saturated aqueous solution.

**NMR Experiments.** All NMR experiments were carried out on a Bruker DSX-400 spectrometer (Karlsruhe, Germany) operating at a resonance frequency of 400.49 MHz for $^1$H, 100.72 MHz for $^{13}$C, and 40.58 MHz for $^{15}$N. A triple-resonance MAS probe with a 4-mm spinning module was used for the experiments. All experiments were conducted at room temperature. A spinning speed of 2.5 kHz was used in the MAS experiments. Typical 90° pulse lengths were 3.5 $\mu$s for $^1$H, 5 $\mu$s for $^{13}$C, and 6 $\mu$s for $^{15}$N. The $^1$H decoupling field strength was about 73 kHz during acquisition and 85 kHz during the CSA evolution. A $^{15}$N decoupling field strength of ~20 kHz was used during the $^{13}$C CSA evolution. CP spin-lock field strength of ~50 kHz was used, and the contact time was 500 $\mu$s except for the C−H modulated CSA experiment. The indirect dimension ($\omega_1$) of the 2D MAS experiments was incremented rotor-synchronously, at 400 $\mu$s per step. Due to the CSA scaling factor of 0.155, the effective $t_1$ dwell time was 400 $\mu$s × 0.155 = 62 $\mu$s, which was used in data processing. Recycle delays of 1.5−3 s were used. Total signal-averaging time for each 2D MAS experiment ranged from 2 to 22 h. Typical line broadening was 220 Hz in the direct dimension ($\omega_2$) and ~150 Hz in the indirect ($\omega_1$) dimension. All $^{13}$C chemical shifts were referenced to the glycine carbonyl line at 176.4 ppm (relative to TMS).

The static 2D C−H dipolar and $^{13}$C CSA correlation experiment[19] was performed with $^1$H homonuclear decoupling during $t_1$, which was accomplished by MREV-8.[23,24] For the 2D C−N/$^{13}$C correlation experiment, a pair of simultaneous $\pi$ pulses on the $^{13}$C and $^{15}$N channels were used during the $t_1$ period to select the C−N dipolar coupling.

**Dipolar-Modulated CSA Experiment.** The orientation of the Cα chemical shift tensor is extracted from C−H and C−N modulated CSA spectra. Basically, the dipolar interactions modulate the CSA spectra according to the relative orientation of each dipolar vector to the CSA tensor. A dipolar-modulated CSA pattern is equivalent to the projection of a 2D SLF spectrum onto the chemical shift dimension after multiplying the dipolar dimension with a modulation function.

To carry out the dipolar-modulation experiment, we first recouple the CSA interaction under MAS to obtain spectra resembling the static powder patterns. This CSA recoupling is achieved using a sequence modified from the four-$\pi$-pulse experiment originally proposed by Tycko and co-workers.[25] In the original experiment, the four $\pi$ pulses were applied at specific time points in a MAS rotation period, such that the time-averaged chemical shift frequency equals the static frequency scaled by a constant factor. However, this experiment is sensitive to pulse imperfections due to rf field inhomogeneity, which give rise to artifacts at the edges of the spectra and broaden the CSA patterns. The improved technique, termed SUPER,[26] replaces the $\pi$ pulses with $2\pi$ pulses in the interval between each pair of $\pi$ pulses (Figure 1a). Thus, instead of inverting the sign of the chemical shift frequency, the $2\pi$ pulses make the frequency vanish to zero. This gives rise to the same recoupling phenomenon except that the scaling factor is reduced by a factor of 2 compared to the $\pi$-pulse-based sequence. More importantly, since the $2\pi$ nutation pulses are much less sensitive to rf field inhomogeneity, and phase cycling further compensates for pulse length and pulse phase errors, the recoupled CSA spectra show much less distortion. In addition, it can be shown that the $^1$H decoupling field strength only needs to be twice stronger than the $^{13}$C field strength during the $2\pi$ pulses,[26] while for $\pi$ pulses the $^1$H field strength has to be 3 times stronger to achieve similarly good decoupling.[27] An important aspect of both the original $\pi$-pulse-based recoupling sequence and the improved SUPER sequence is that the recoupled CSA frequency depends on the orientations of the individual molecules relative to the magnetic field in the laboratory frame at the beginning of the rotor period. To modulate the CSA powder pattern with a dipolar coupling,

(15) deDios, A. C.; Pearson, J. G.; Oldfield, E. *Science* **1993**, *260*, 1491−1496.
(16) Naito, A.; Ganapathy, S.; Akasaka, K.; McDowell, C. A. *J. Chem. Phys.* **1981**, *74*, 3190−3197.
(17) Haberkorn, R. A.; Stark, R. E.; Willigen, H. v.; Griffin, R. G. *J. Am. Chem. Soc.* **1981**, *103*, 2534−2539.
(18) Hester, R. K.; Ackermann, J. L.; Neff, B. L.; Waugh, J. S. *Phys. Rev. Lett.* **1976**, *36*, 1081.
(19) Linder, M.; Hoehener, A.; Ernst, R. R. *J. Chem. Phys.* **1980**, *73*, 4959−4970.
(20) Munowitz, M. G.; Griffin, R. G.; Bodenhausen, G.; Huang, T. H. *J. Am. Chem. Soc.* **1981**, *103*, 2529−2533.
(21) Ishii, Y.; Terao, T.; Kainosho, M. *Chem. Phys. Lett.* **1996**, *256*, 133−140.
(22) Greenstein, J. P.; Milton, W. *Chemistry of the Amino Acids*; Wiley: New York, 1961.
(23) Rhim, W.-K.; Elleman, D. D.; Vaughan, R. W. *J. Chem. Phys.* **1973**, *59*, 3740−3749.
(24) Mansfield, P. *J. Phys. Chem.* **1971**, *4*, 1444.
(25) Tycko, R.; Dabbagh, G.; Mirau, P. *J. Magn. Reson.* **1989**, *85*, 265−274.
(26) Liu, S. F.; Mao, J. D.; Schmidt-Rohr, K. *J. Magn. Reson.* **2002**. In press.
(27) Ishii, Y.; Ashida, J.; Terao, T. *Chem. Phys. Lett.* **1995**, *246*, 439−445.

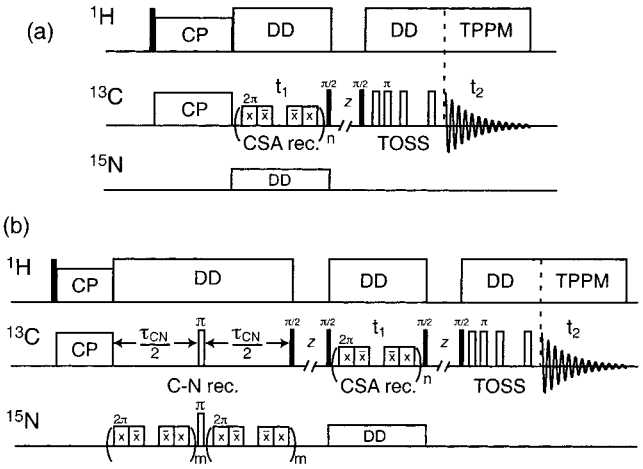


***Figure 1.*** Pulse sequences for dipolar-modulated CSA recoupling experiments to determine the chemical shift tensor orientation. (a) CSA recoupling experiment. With a short $^1$H−$^{13}$C CP contact time, this becomes the C−H modulation experiment. (b) C−N modulation experiment. DD, dipolar decoupling; TOSS, total sideband suppression; TPPM, two-pulse phase modulation.

one must ensure that the dipolar frequency is expressed in the same coordinate frame as the recoupled CSA interaction, which is the laboratory frame. The simplest C−H modulation scheme in the laboratory frame is cross polarization (CP).[28] For an isolated two-spin system containing a $^1$H and a $^{13}$C, the magnetization of the $^{13}$C ($C_X$) depends on the CP contact time $\tau_{CH}$ according to

$$C_X\frac{1}{2}(1 - \cos\omega_{CH}\tau_{CH}) = C_X\sin^2(\omega_{CH}\tau_{CH}) \quad (1)$$

where $\omega_{CH}$ is the orientation-dependent dipolar coupling between the $^1$H and $^{13}$C spins.[29,30] This time dependence modulates the CSA spectra recoupled during the subsequent $t_1$ period. When a CP time much shorter than the sample rotation period is used, the C−H dipolar coupling can be approximated as quasi-static. Thus, its modulation of the CSA spectra is completely determined by the relative orientation of the CSA tensor and the C−H dipolar vector. Further, a short CP time limits the heteronuclear dipolar coupling to the nearest-neighbor $^{13}$C and $^1$H spins, so that only the desired one-bond Cα−Hα coupling will modulate the Cα chemical shift powder pattern.

At a spinning speed of 2.5 kHz, we used a $^1$H−$^{13}$C CP contact time of 20 μs. The sample rotates by 18° during this time. Numerical simulations of the orientation-dependent dipolar frequency indicate that, for a rotor phase change of 18°, the powder-averaged absolute-value frequency change is less than 16% of the dipolar coupling constant. Thus, the quasi-static approximation of the C−H dipolar coupling under this combination of short CP and slow spinning is valid. In contrast, with a long $\tau_{CH}$ time, as is typical for a normal CP experiment, both the quasi-static and two-spin approximations break down; thus, the chemical shift powder pattern will no longer be modulated by the simple time-independent two-spin dipolar couplings. The SUPER sequence recouples any anisotropic interactions that are linear in the irradiated spin. Thus, applied to $^{13}$C, the sequence reintroduces not only the $^{13}$C CSA but also the $^{13}$C−$^{15}$N dipolar coupling. To selectively observe the $^{13}$C CSA spectra, the $^{15}$N spins are decoupled from $^{13}$C by continuous irradiation. This is shown in Figure 1a for the evolution period. After the evolution period, a *z*-filter is applied on $^{13}$C to store the cosine and sine components of the $t_1$ signals separately. They are then combined according to the States method[31] to obtain pure absorptive spectra in the $\omega_1$ dimension. Before detection, a total sideband suppression (TOSS) pulse train[32] is inserted to remove spinning sidebands in the $\omega_2$ dimension.

The pulse sequence for measuring the relative orientation of the CSA tensor with respect to the C−N bond is shown in Figure 1b. The $^{13}$C−$^{15}$N dipolar interaction is recoupled by applying the SUPER sequence on the $^{15}$N channel, combined with a pair of simultaneous $\pi$ pulses on the $^{13}$C and $^{15}$N channels in the middle of the C−N dephasing period, $\tau_{CN}$. This combination refocuses the $^{13}$C and $^{15}$N chemical shift interaction, while preserving the $^{13}$C−$^{15}$N dipolar coupling. The $^{13}$C magnetization evolves under this recoupled C−N dipolar interaction for a constant period $\tau_{CN}$. A *z*-filter at the end of $\tau_{CN}$ selects the cosine-modulated $^{13}$C magnetization, $C_X\cos(\omega_{CN}\tau_{CN})$, which then evolves under the $^{13}$C CSA interaction during $t_1$. Thus, the 2D experiment yields recoupled CSA patterns modulated by $\cos(\omega_{CN}\tau_{CN})$ in the $\omega_1$ dimension, separated according to the isotropic chemical shift of each $^{13}$C in the $\omega_2$ dimension.

The requirement of having two $2\pi$ pulses in a fixed time interval constrains the rf field strength ($\omega_{1C}$) of the $^{13}$C recoupling pulses. In our experiments, we used the timing $0.089\tau_r$ and $0.254\tau_r$ for the boundaries of the first pair of $2\pi$ pulses, and $0.746\tau_r$ to $0.911\tau_r$ for the second pair of $2\pi$ pulses, where $\tau_r$ is the sample rotation period. As a result, $\omega_{1C}$ is 12.12 times the spinning speed, $\omega_r$. Meanwhile, the $^{13}$C field strength must be significantly lower than the $^1$H decoupling field strength in order to avoid reverse CP. The finite $^1$H decoupling field strength thus constrains the spinning speed. For all experiments shown here, the samples were spun at 2.5 kHz, which corresponded to $\omega_{1C}$ = 30.3 kHz. The $^1$H decoupling field strength was typically ∼85 kHz, which is sufficiently higher than the $^{13}$C rf field strength to minimize the $^{13}$C signal loss. This moderate spinning speed justifies the use of the TOSS sequence before detection. The CSA scaling factor corresponding to this pulse timing is 0.155.

**Simulation.** To extract the relative orientation of the chemical shift tensor to the dipolar vectors, the C−H and C−N modulated CSA spectra were simulated in the frequency domain using Fortran programs. The programs calculate the 2D SLF spectra as a function of the polar angle and azimuthal angle of the uniaxial dipolar tensor in the chemical shift principal axis system (PAS). The spectrum was then multiplied by the appropriate modulation function in the $\omega_1$ dimension and projected onto the chemical shift, or $\omega_2$, dimension. The equivalence between this projected SLF spectrum and the experimental dipolar-modulated recoupled CSA spectrum can be shown as follows for the C−N modulation experiment:

$$\int S(\omega_{CN},\omega_2)\cos(\omega_{CN}\tau_{CN})\,d\omega_{CN} = \mathrm{Re}[\int S(\omega_{CN},\omega_2)e^{i\omega_{CN}\tau_{CN}}\,d\omega_{CN}] = \mathrm{Re}[S(\tau_{CN},\omega_2)] \quad (2)$$

Similarly, the C−H modulated CSA spectrum is identical to the projection of the 2D static C−H/$^{13}$C correlation spectrum multiplied by $\sin^2(\omega_{CH}\tau_{CH})$ in the $\omega_1$ dimension.

The relative orientations of the CSA tensor and the Cα−X (X = $^1$H or $^{15}$N) dipolar tensor can be described in terms of the direction angles, $\beta_{CX}(\sigma_{ii})$, between the C−X vector and the three CSA principal axes $\sigma_{ii}$ ($i$ = 1, 2, 3). However, in the simulations, the orientation of the dipolar vector in the chemical shift PAS is varied more conveniently in terms of the polar angle $\beta_{CX}(\sigma_{ii})$ and azimuthal angle $\alpha_{CX}(\sigma_{ii})$. These polar coordinates are related to the direction angles in a well-defined fashion. For example, $\cos\beta_{CN}(\sigma_{11}) = \cos(\alpha_{CN}(\sigma_{33}))\sin(\beta_{CN}(\sigma_{33}))$. The three chemical shift principal axes are arranged in a right-handed coordinate system, with the *z*-axis indicated by $\sigma_{ii}$ in the bracket of $\beta$ and α angles and the *x*-axis corresponding to $\alpha_{CX}(\sigma_{ii}) = 0°$. For instance, $\alpha_{CH}(\sigma_{11})$

(28) Pines, A.; Gibby, M. G.; Waugh, J. S. *J. Chem. Phys.* **1973**, *59*, 569−590.
(29) Schmidt-Rohr, K.; Spiess, H. W. *Multidimensional Solid-State NMR and Polymers*, 1st ed.; Academic Press: San Diego, 1994.
(30) Mehring, M. *High-Resolution NMR in Solids*; Springer-Verlag: New York, 1983.
(31) States, D. J.; Haberkorn, R. A.; Ruben, D. J. *J. Magn. Reson.* **1982**, *48*, 286−292.
(32) Dixon, W. T. *J. Chem. Phys.* **1982**, *77*, 1800−1809.

is the azimuthal angle of the C−H bond in a PAS system where $\sigma_{11}$ is along the *z*-direction, $\sigma_{22}$ is along the *x*-axis, and $\sigma_{33}$ is along the *y*-axis.

For methylmalonic acid, we specified the orientation of the most deshielded element, $\sigma_{11}$, with respect to the C−H bond, while for *N*-tBoc-glycine, the orientation of the most shielded principal axis, $\sigma_{33}$, was specified relative to the Cα−N bond. For the model peptide NAV, we defined the CSA tensor orientation in terms of the angle between the $\sigma_{11}$ principal axis and the Cα−Hα bond and the angle between the $\sigma_{22}$ axis and the Cα−N bond. This follows the angle definitions of Havlin et al.,[5] thus facilitating comparison with the quantum chemical calculations. For the NAV measurements, we mainly focus our analysis on the polar angles $\beta_{CH}(\sigma_{11})$ and $\beta_{CN}(\sigma_{22})$. The corresponding azimuthal angles, $\alpha_{CH}(\sigma_{11})$ and $\alpha_{CN}(\sigma_{22})$, are useful for constraining the orientation of the $\sigma_{33}$ axis relative to the Cα−CO bond.

In the simulations, powder averaging was achieved using 720 angular steps. Due to the invariance of NMR frequencies to vector inversion, the spectra have a 2-fold degeneracy in a 180° range for both α and $\beta$ angles. Thus, the simulations were carried out only in the range 0°−90°. This angular range was scanned with a resolution of 5°. Near the best fit to the experiment, the simulations were carried out at 1° increments. The one-bond $^{13}C-^{1}H$ and $^{13}C-^{15}N$ dipolar couplings were 22 and 1 kHz, respectively. The simulated and experimental spectra were normalized so that the maximum intensity is 1. The normalized spectra were compared, and the best fits were obtained from the minimum root-mean-square deviations (RMSD) between the experimental spectrum, $S_{exp}$, and the simulated spectra, $S_{sim}^{\alpha,\beta}$ according to

$$\mathrm{RMSD}(\alpha,\beta) = \sqrt{\sum_{i=1}^{n}(S_{sim}^{\alpha,\beta}(i) - S_{exp}(i))^2/n} \qquad (3)$$

where *n* is the number of points in each spectrum.

## Results and Discussion

**C−H Modulated CSA Experiment on Methylmalonic Acid.** Methylmalonic acid is an ideal model compound to demonstrate the C−H modulated CSA technique. It contains a CH, a $CH_3$, and a COO group, whose isotropic and anisotropic chemical shifts are sufficiently different that the three $^{13}C$ signals are resolved even in a static powder spectrum. This allows us to compare the recoupled CSA spectra under MAS with the static spectra without using a $^{13}C$-labeled sample.

Figure 2a shows the recoupled CSA pattern of the methine (CH) carbon, extracted from a 2D spectrum acquired with a CP contact time of 500 μs. The powder pattern does not have any intensity suppression, and simulation yielded principal values of 59.7, 49.7, and 30.2 ppm. This recoupled CSA spectrum agrees very well with the 1D static powder pattern in Figure 2b. Due to the isotropic shift separation by the 2D experiment, the recoupled CSA spectrum contains no neighboring $CH_3$ signal, in contrast to the static spectrum.

When the $^{1}H-^{13}C$ CP time was reduced to 20 μs, the intensities of the MAS spectrum (Figure 2c) became significantly attenuated around 40 ppm, while the intensities around $\sigma_{11}$ remained high. This agrees qualitatively with the static spectrum acquired with the same CP time (Figure 2d). Again, the static spectrum shows the methyl $^{13}C$ signal that is absent in the CH cross section of the site-resolved 2D MAS spectrum. Due to the C−H modulation, $\sin^2(\omega_{CH}\tau_{CH})$, the CSA spectrum should exhibit the highest intensity at the principal value whose axis is most parallel to the C−H bond. When the two interaction axes are collinear, a crystallite whose chemical shift principal axis is along the external magnetic field also has the C−H bond parallel to the field. Thus, that crystallite has the largest dipolar coupling, and the modulation function $\sin^2(\omega_{CH}\tau_{CH})$ acquires the maximum value at short $\tau_{CH}$. This interpretation of the C−H modulated CSA spectra is confirmed by the simulations in Figure 3. For $\beta_{CH}(\sigma_{11}) = 0°$, the $\sigma_{11}$ edge of the modulated CSA spectra is preferentially enhanced. Varying the azimuthal angle $\alpha_{CH}(\sigma_{11})$ does not affect the spectra, since the C−H bond always has the same projection onto the transverse plane. As $\beta_{CH}(\sigma_{11})$ increases toward 90°, the $\sigma_{11}$ intensity decreases, and the $\alpha_{CH}(\sigma_{11})$ degeneracy is removed. When $\beta_{CH}(\sigma_{11}) = 90°$ and $\alpha_{CH}(\sigma_{11}) = 0°$, the C−H bond becomes parallel to the $\sigma_{22}$ axis; thus, the $\sigma_{22}$ edge of the spectrum exhibits maximum intensity. The experimental spectrum of methylmalonic acid (Figure 2c) is best fit by $\beta_{CH}(\sigma_{11}) = 25°$ and $\alpha_{CH}(\sigma_{11}) = 20°$.

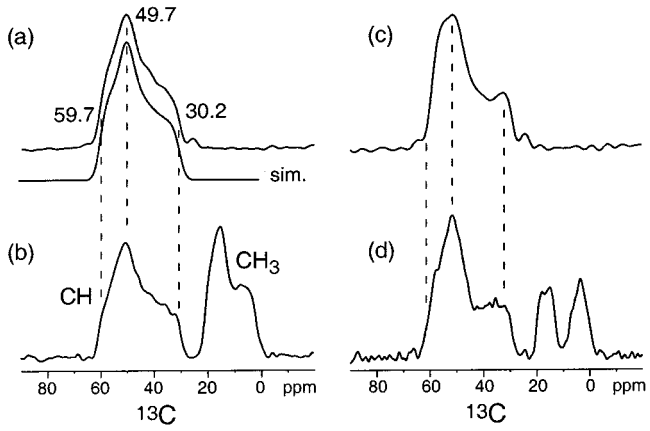


***Figure 2.*** C−H modulated CSA spectra of methylmalonic acid. (a) Recoupled CSA spectrum of the methine carbon, extracted from the 2D spectrum at the isotropic shift of the methine carbon. CP contact time, 500 μs. Best-fit simulation is shown below the experimental spectrum and gives the principal values of the chemical shift tensor. The 2D spectrum was obtained in 2 h with 64 scans per $t_1$ slice. (b) 1D static $^{13}C$ spectrum, acquired with a CP contact time of 500 μs. Number of scans (NS) = 512. (c) Recoupled CSA spectrum of the methine carbon, acquired with a CP contact time of 20 μs. NS per $t_1$ slice, 96. (d) 1D static $^{13}C$ spectrum, acquired with a CP contact time of 20 μs. NS = 128. Both 2D MAS spectra (a, c) were recorded with 48 $t_1$ slices and a maximum evolution time of 9.6 ms.

To confirm the result of this MAS experiment, we measured the 2D SLF spectrum of methylmalonic acid, correlating the C−H dipolar coupling with the $^{13}C$ CSA. The natural separation of the three $^{13}C$ signals in this compound allowed us to analyze the methine carbon powder pattern without resonance overlap. The $^{1}H-^{13}C$ dipolar dimension was recorded with $^{1}H$ homonuclear decoupling during the evolution period. The largest $^{1}H-^{13}C$ splitting was observed close to the most downfield component, $\sigma_{11}$, of the spectrum. This is consistent with the high intensity of the $\sigma_{11}$ edge at short CP times. Between $\sigma_{22}$ and $\sigma_{33}$, a ridge of roughly constant dipolar splitting that corresponds to about half the rigid-limit coupling was detected. This indicates that the C−H bond is approximately perpendicular to the $\sigma_{33}$ and $\sigma_{22}$ axes. Indeed, the best-fit simulation of the 2D spectrum yielded $\beta_{CH}(\sigma_{11}) = 25°$ and $\alpha_{CH}(\sigma_{11}) = 10°$, in good agreement with the MAS result. The best-fit 2D spectrum differs significantly from other orientations of the chemical shift tensor, as shown by the simulated spectra for $\beta_{CH}(\sigma_{11}) = 60°$ and $\beta_{CH}(\sigma_{11}) = 90°$, both with $\alpha_{CH}(\sigma_{11}) = 0°$ (Figure 4c,d).

**C−N Modulated CSA Experiment on $^{15}N$-tBoc-$^{13}C\alpha$-glycine.** We chose *N*-tBoc-glycine, one of the few commercially

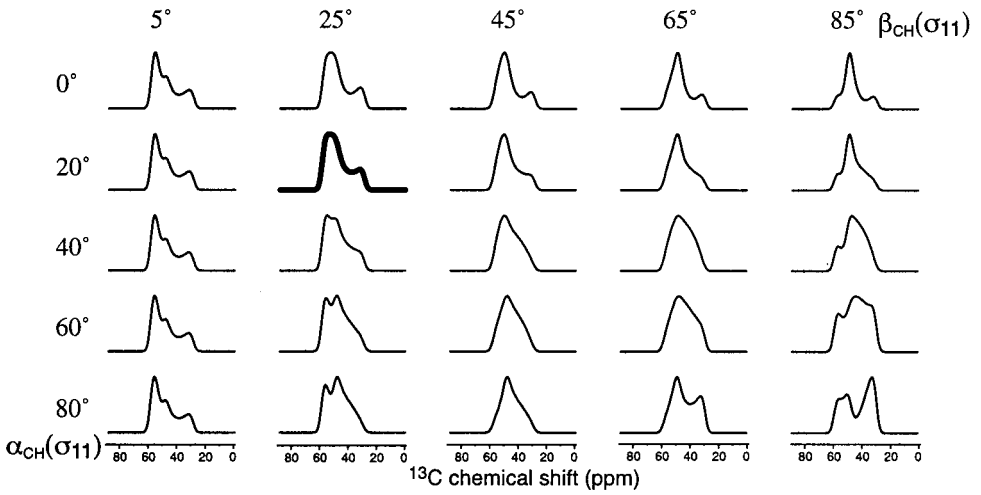


***Figure 3.*** Simulated C−H modulated CSA spectrum of the methine carbon in methylmalonic acid, using the principal values obtained from the simulation in Figure 2a. Columns show variations with the polar angle, $\beta_{CH}(\sigma_{11})$, between the $\sigma_{11}$ axis and the C−H bond. Rows show variations with the corresponding azimuthal angle, $\alpha_{CH}(\sigma_{11})$. The best-fit simulation, with $\beta_{CH}(\sigma_{11}) = 25°$ and $\alpha_{CH}(\sigma_{11}) = 20°$, is shown in bold.

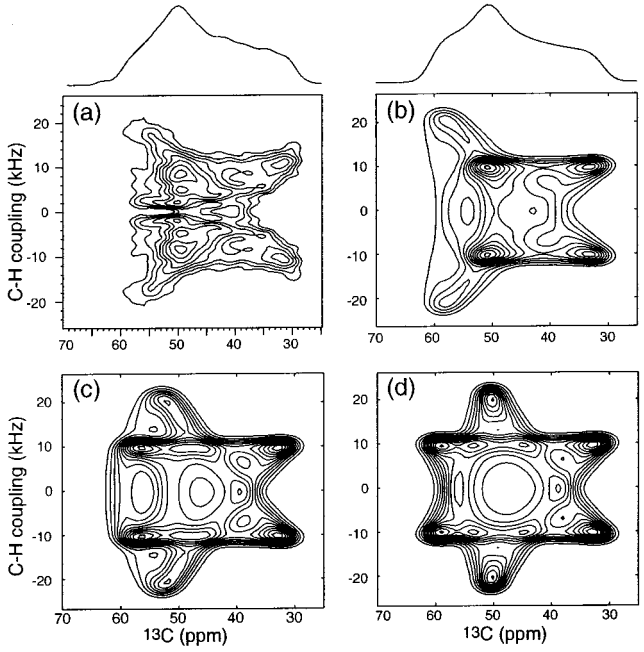


***Figure 4.*** (a) 2D separated-local-field spectrum of methylmalonic acid, correlating the C−H dipolar coupling with the $^{13}$C chemical shift anisotropy. Only the methine region is shown. The spectrum was acquired in 8 h with 768 scans per $t_1$ slice, 16 $t_1$ slices, and a maximum evolution time of 614 $\mu$s. (b) Best-fit simulation, obtained with $\beta_{CH}(\sigma_{11}) = 25°$ and $\alpha_{CH}(\sigma_{11}) = 10°$. (c) Simulation with $\beta_{CH}(\sigma_{11}) = 60°$ and $\alpha_{CH}(\sigma_{11}) = 0°$. (d) Simulation with $\beta_{CH}(\sigma_{11}) = 90°$ and $\alpha_{CH}(\sigma_{11}) = 0°$.

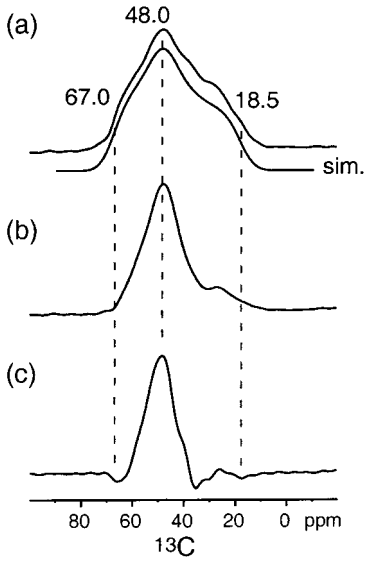


***Figure 5.*** C−N modulated CSA spectra of $^{15}N$-tBoc-$^{13}$Cα-glycine. (a) Recoupled Cα CSA spectrum without dipolar dephasing. Best-fit simulation is shown below the experimental spectrum. NS per $t_1$ slice, 16. (b) Recoupled Cα CSA spectrum with 3.2 ms of C−N dipolar dephasing. NS per $t_1$ slice, 96. (c) Recoupled Cα CSA spectrum with 4.0 ms of C−N dipolar modulation. NS per $t_1$ slice, 128. All 2D spectra were recorded with 50 $t_1$ slices and a maximum evolution time of 10 ms.

available amino acids with $^{15}$N and $^{13}$Cα double labeling, to demonstrate the measurement of the orientation of the Cα CSA tensor relative to the C−N bond. Figure 5a shows the unmodulated Cα CSA spectrum of *N*-tBoc-glycine, extracted from the Cα cross section of the 2D MAS spectrum. The best-fit simulation yielded principal values of $\sigma_{11} = 67.0$ ppm, $\sigma_{22} = 48.0$ ppm, and $\sigma_{33} = 18.5$ ppm. The $^{13}$C−$^{15}$N dipolar dephasing was then turned on for 3.2 ms and for 4.0 ms, yielding spectra in Figure 5b and 5c, respectively. Since the modulation function is $\cos(\omega_{CN}\tau_{CN})$, the frequency position with the lowest intensity, rather than maximal intensity, is most parallel to the C−N bond. Simple inspection of the experimental spectra indicates that the C−N bond must lie somewhere between the most shielded element, $\sigma_{33}$, and the intermediate $\sigma_{22}$ axis.

Simulated CSA spectra with 4 ms of C−N dephasing are displayed in Figure 6. Large negative intensities are observed near the $\sigma_{33}$ edge for $\beta_{CN}(\sigma_{33})$ around 0° and close to the $\sigma_{11}$ edge for $\beta_{CN}(\sigma_{33})$ near 90° and $\alpha_{CN}(\sigma_{33})$ near 0°. At $\beta_{CN}(\sigma_{33}) = \alpha_{CN}(\sigma_{33}) = 90°$, the C−N bond is parallel to the $\sigma_{22}$ axis; thus, the center of the powder pattern shows the most negative intensities. The best-fit simulation yielded $\beta_{CN}(\sigma_{33}) = 35°$ and $\alpha_{CN}(\sigma_{33}) = 90°$, consistent with the expectation that the C−N bond lies between the $\sigma_{33}$ and the $\sigma_{22}$ axis. The result of this C−N modulated CSA recoupling experiment was verified by a 2D static SLF spectrum correlating the $^{13}$C−$^{15}$N dipolar coupling with the $^{13}$C CSA. The 2D spectrum (Figure 7a) shows the largest splitting close to the $\sigma_{33}$ edge of the powder pattern,

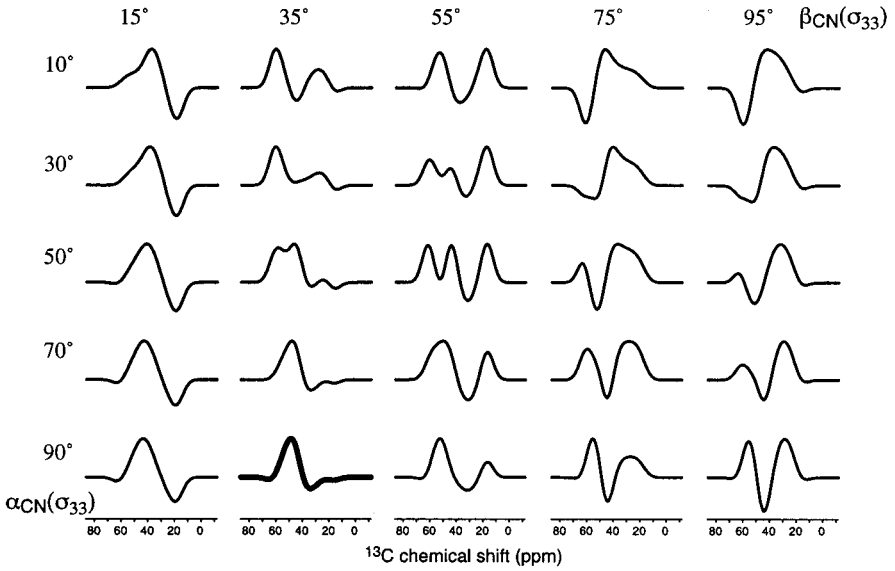


***Figure 6.*** Simulated C−N modulated CSA spectra of the Cα site of *N*-tBoc-glycine. Spectra vary as a function of angles $\beta_{CN}(\sigma_{33})$ and $\alpha_{CN}(\sigma_{33})$ between the $\sigma_{33}$ axis and the C−N bond. The best-fit simulation, obtained with $\beta_{CN}(\sigma_{33}) = 35°$ and $\alpha_{CN}(\sigma_{33}) = 90°$, is shown in bold.

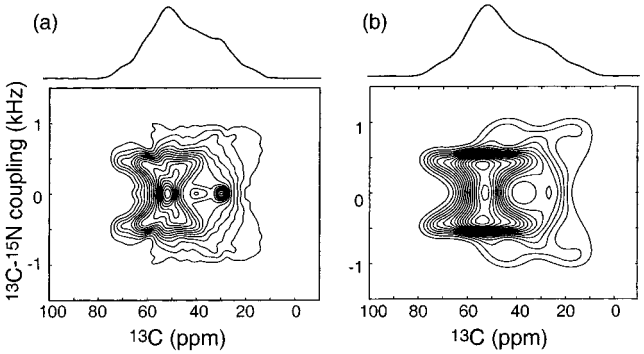


***Figure 7.*** (a) 2D SLF spectrum of *N*-tBoc-glycine, correlating the $^{13}C-^{15}N$ dipolar coupling with the $^{13}C$ chemical shift anisotropy. The spectrum was acquired in 20 min with 16 scans per $t_1$ slice, 32 slices, and a maximum evolution time of 4 ms. (b) Best-fit simulation: $\beta_{CN}(\sigma_{33}) = 35°$ and $\alpha_{CN}(\sigma_{33}) = 80°$.

while the downfield edge, $\sigma_{11}$, has about half the rigid-limit splitting. The best-fit simulation (Figure 7b) yielded angles of $\beta_{CN}(\sigma_{33}) = 35°$ and $\alpha_{CN}(\sigma_{33}) = 80°$, in good agreement with the MAS results.

**Cα Chemical Shift Tensor Orientation of *N*-Acetyl-D,L-valine.** Using these two dipolar-modulated CSA techniques, we measured the Cα tensor orientation of $^{15}N$-acetylvaline, a compound with torsion angles of $\phi = -136.5°$ and $\psi = 180°$ for the Val residue, as determined by X-ray crystallography.[33] Figure 8a shows the unmodulated CSA pattern and its best-fit simulation. The principal values are 82.6, 53.2, and 36.1 ppm. The C−H modulated spectrum, acquired with a CP contact time of 20 $\mu$s (Figure 8b), shows that the intensity is best retained near the $\sigma_{11}$ edge of the powder pattern, indicating that the C−H bond is approximately parallel to the $\sigma_{11}$ axis. The C−N modulated CSA spectrum with 4.0 ms of dipolar dephasing (Figure 8c) exhibits two distinct valleys, which correspond to the largest C−N dipolar coupling.

The quantitative orientation of the Cα chemical shift tensor relative to the C−H bond is obtained from simulations in Figure 9. The simulations were carried out as a function of the angles between the C−H bond and $\sigma_{11}$ axis to facilitate later comparison with quantum chemical calculations.[5] When $\beta_{CH}(\sigma_{11}) = 0°$, the most downfield edge of the powder pattern has the highest intensity. When $\beta_{CH}(\sigma_{11}) = 90°$ and $\alpha_{CH}(\sigma_{11}) = 90°$, the C−H bond is aligned with the $\sigma_{33}$ axis, giving the upfield edge of the spectrum the highest intensity. Finally, when $\beta_{CH}(\sigma_{11}) = 90°$ and $\alpha_{CH}(\sigma_{11}) = 0°$, the C−H bond is aligned with the $\sigma_{22}$ axis, thus enhancing the intensity in the middle of the spectrum. The

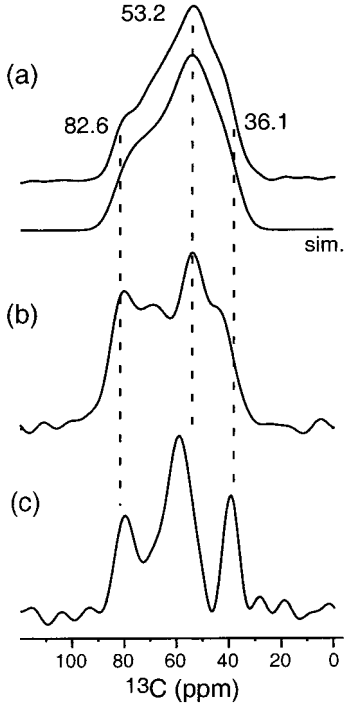


***Figure 8.*** Recoupled CSA spectra of $^{15}N$-acetylvaline. (a) Without dipolar modulation. NS per $t_1$ slice, 256. The best-fit simulation is shown below the experimental spectrum. (b) C−H modulated CSA spectrum, acquired with a CP contact time of 20 $\mu$s. NS per $t_1$ slice, 256. (c) C−N modulated CSA spectrum, acquired with a C−N dephasing time of 4.0 ms. NS per $t_1$ slice, 512. All 2D spectra were obtained with 40 $t_1$ slices and a maximum evolution time of 8 ms, except for spectrum b, which was processed using 36 $t_1$ slices.

(33) Carroll, P. J.; Stewart, P. L.; Opella, S. J. *Acta Crystallogr.* **1990**, *C46*, 243−246.

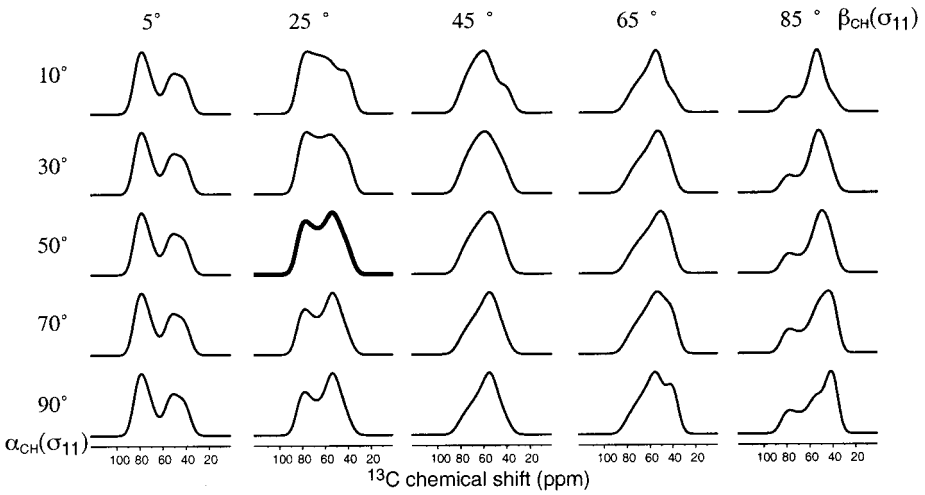


***Figure 9.*** Simulated C−H modulated CSA spectra of NAV as a function of the angles between the $\sigma_{11}$ axis and the C−H bond. The simulation closest to the best-fit of $\beta_{CH}(\sigma_{11}) = 22°$ and $\alpha_{CH}(\sigma_{11}) = 58°$ is shown in bold.

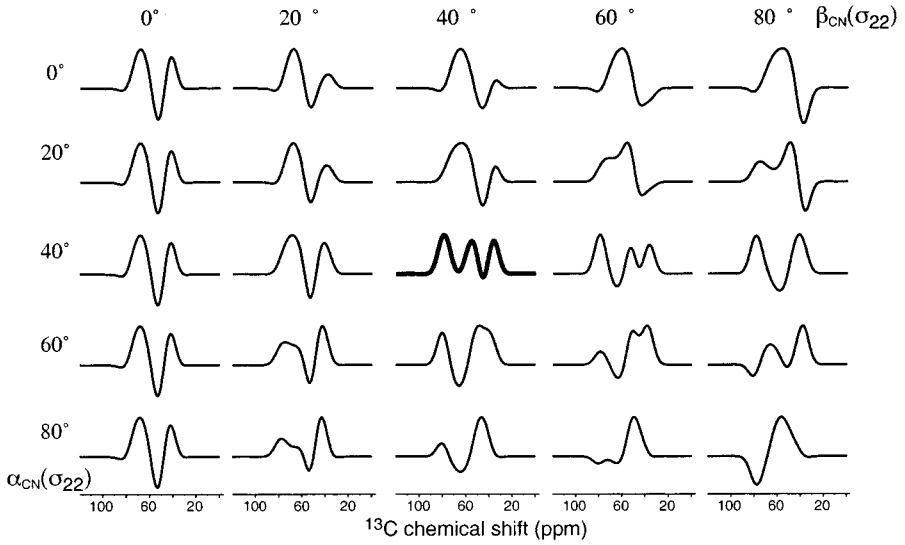


***Figure 10.*** Simulated C−N modulated CSA spectra of NAV as a function of the angles between the $\sigma_{22}$ axis and the C−N bond. The simulation closest to the best fit of $\beta_{CN}(\sigma_{22}) = 36°$ and $\alpha_{CN}(\sigma_{22}) = 37°$ is shown in bold.

best-fit simulation, as determined by the RMSD calculation described below, yields $\beta_{CH}(\sigma_{11}) = 22°$ and $\alpha_{CH}(\sigma_{11}) = 58°$. Thus, the $\sigma_{11}$ axis of the Cα chemical shift tensor is approximately along the C−H bond. The small deviation between the experiment and the best fit is most likely a result of the signal-to-noise ratio of the experimental spectrum.

A similar set of simulations, made by varying the orientation of the C−N bond relative to the $\sigma_{22}$ axis, was carried out for the C−N modulated CSA experiment (Figure 10). The experimental spectrum was best reproduced by $\beta_{CN}(\sigma_{22}) = 36°$ and $\alpha_{CN}(\sigma_{22}) = 37°$.

To quantify the angular precision of the NAV Cα tensor orientation, we calculated the RMSDs between each experimental dipolar-modulated CSA spectrum and the corresponding simulations. This is shown as two contour plots in Figure 11. The minimum RMSD value was normalized to 1, and 15 contour lines were plotted between the maximum and minimum RMSD values. The RMSD plot for the C−H modulation experiment shows that the spectra are extremely sensitive to the polar angle $\beta_{CH}(\sigma_{11})$ but less sensitive to the azimuthal angle $\alpha_{CH}(\sigma_{11})$. The C−N modulated spectra show comparable angular resolution in both the α and $\beta$ angles. For both experiments, the best-fit simulation is significantly better than the rest, as indicated by the relatively steep contour level changes at the global minimums. We estimate the uncertainty in the measured polar angles, $\beta_{CH}(\sigma_{11})$ and $\beta_{CN}(\sigma_{22})$, to be 3°, while the uncertainty in the two azimuthal angles are about 10° for the C−H experiment and 5° for the C−N experiment. Thus, the angular resolution of these dipolar-modulation experiments is reasonably high.

Figure 11 also shows the angular degeneracy of these dipolar-modulated CSA experiments. Both the $\beta$- and α angles have a 2-fold degeneracy within a 180° range. This means that $\beta$ and $180° - \beta$, or α and $180° - \alpha$, are equally valid solutions. Overall, eight pairs of equivalent solutions can be found, since the $\beta$ angle varies from 0° to 180° and the α angle varies from 0° to 360°.

**Comparison of Experimental NAV Tensor with Quantum Chemical Calculations.**

Figure 12 summarizes the orientation of the Cα chemical shift tensor of NAV. The $\sigma_{11}$ axis is drawn to be 158° from the C−H bond, while the $\sigma_{22}$ axis is 144° from the C−N bond. We chose these values instead of the complementary values of 22° and

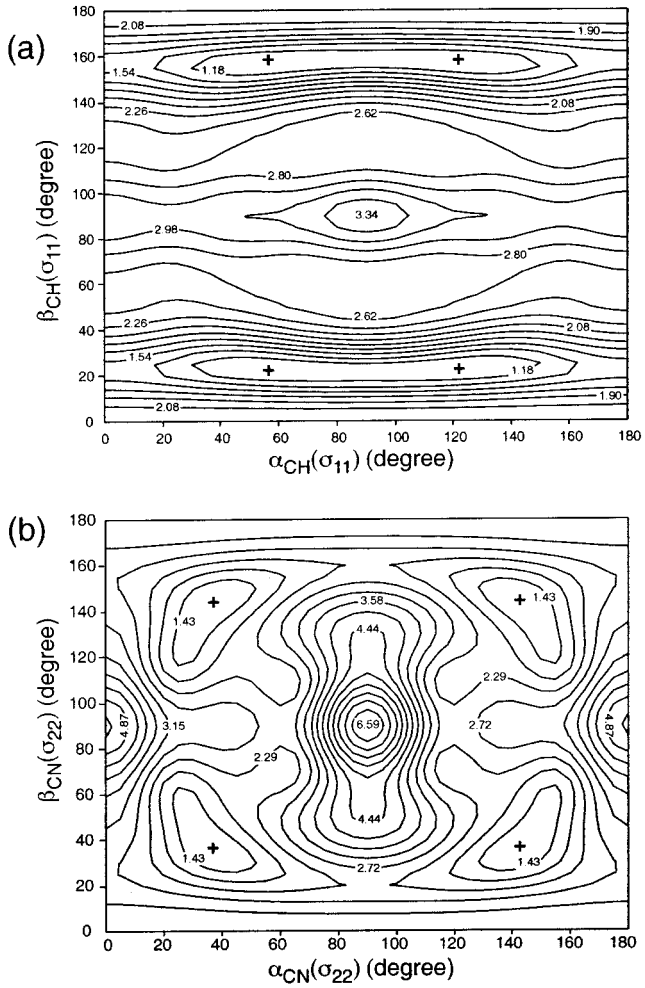


***Figure 11.*** Plots of RMSDs between the experimental NAV spectra and the simulations. (a) $^{13}C-^{1}H$ modulated CSA experiment. The minimum RMSD (cross) is found for $\beta_{CH}(\sigma_{11}) = 22°$, $\alpha_{CH}(\sigma_{11}) = 58°$, and their complementary angles. (b) $^{13}C-^{15}N$ modulated CSA experiment. The minimum RMSD is found for $\beta_{CN}(\sigma_{22}) = 36°$, $\alpha_{CN}(\sigma_{22}) = 37°$, and their complementary angles.

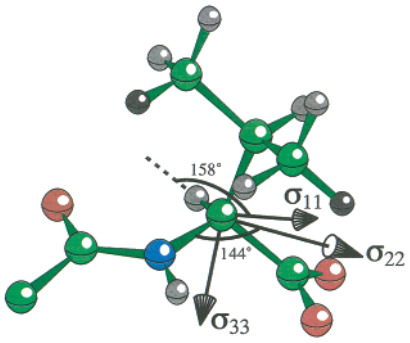


***Figure 12.*** Orientation of the Cα chemical shift tensor of Val in NAV. The angles between the $\sigma_{11}$ axis and the C−H bond and between the $\sigma_{22}$ axis and the C−N bond are indicated. The $\sigma_{33}$ orientation is not measured but has a restricted number of solutions based on the C−H and C−N modulation results.

36°, since they are the closest to the ab initio calculation for *N*-formylvaline amide.[5] The experimental chemical shift parameters for NAV are listed in Table 1, along with the torsion angles of Val determined by X-ray crystallography.[33] For comparison, the quantum-chemical calculated Val chemical shifts for similar torsion angles are also listed. It can be seen

***Table 1.*** The Cα Chemical Shift Tensor of Val in the β-Sheet Conformation

| structure | experimental | calculation[a] |
|---|---|---|
| $\phi^b$ | −136.5° | −135° |
| $\psi^b$ | 178.2° | 180° |
| $\chi_1 b$ | −60° | −60° |
| $\Delta\sigma$ | 46.5 ppm | 45.4 ppm |
| $\eta$ | 0.68 | 0.68 |
| $\sigma_{11}$−CH angle | 22°, 158° | 168° |
| $\sigma_{22}$−CN angle | 36°, 144° | 144° |

[a] The calculation was done for *N*-formylvaline amide and available from ref 5 and the web site http://feh.scs.uiuc.edu/amino_acid.html. [b] The NAV torsion angles were obtained from ref 33.

that the experimental CSA magnitudes, in terms of both the span, $\Delta\sigma = |\sigma_{11} - \sigma_{33}|$, and the asymmetry parameter, $\eta$, are in excellent agreement with the calculations. In terms of the tensor orientation, the theoretical orientation of the $\sigma_{11}$ axis to the C−H bond is only 10° different from the experimental value, while the calculated $\sigma_{22}$ orientation from the C−N bond is identical to the experimental result within the experimental uncertainty. The small difference in the $\sigma_{11}$ orientation could result from the different C-terminus environment of the two molecules: the Val in NAV has a carboxyl end group, while the Val in *N*-formylvaline amide has a carbonyl group capped by a peptide bond. The replacement of a nitrogen atom by an oxygen atom may affect the electronic environment of Cα sufficiently to account for this small difference in $\sigma_{11}$ orientation. Overall, the experiment confirms the calculation that the $\sigma_{11}$ axis is roughly parallel to the C−H bond.

It is reassuring to note that, among the multiple solutions for the four angles obtained from the C−H and C−N dipolar-modulation experiments, a subset is consistent both with the H−C−N bond angle and with the quantum-chemical $\beta_{CH}(\sigma_{11})$ and $\beta_{CN}(\sigma_{22})$ angles. In addition, the orientation of the $\sigma_{33}$ axis relative to the $^{13}C\alpha-^{13}CO$ bond, while not measured here, is constrained by the four measured angles. Due to the degeneracy of the experimentally obtained orientation angles, a number of solutions for $\beta_{CC}(\sigma_{33})$ is found, some of which are ±11° from the predicted angle of 27° in β-sheet Val.

## Conclusions

We have shown a new technique for determining chemical shift tensor orientations in powder samples with site resolution. Static-like CSA powder patterns are recoupled under MAS using a $2\pi$-pulse-based sequence.[26] Site resolution is obtained by correlating the recoupled CSA powder patterns with the isotropic shifts in a 2D fashion. By modulating the recoupled CSA spectra with C−H and C−N dipolar couplings, we obtain the relative orientations of the CSA tensor with respect to these dipolar vectors. The C−H modulation is achieved by use of a short $^{1}H-^{13}C$ CP time, while the C−N modulation is accomplished by dephasing the $^{13}C$ magnetization with the recoupled C−N dipolar interaction. The C−H and C−N modulated CSA experiments were demonstrated on methylmalonic acid and on *N*-tBoc-glycine, respectively. Comparison with the corresponding static SLF spectra indicates that the MAS experiments yield accurate orientation angles. Using these dipolar-modulated CSA methods, we measured the Cα tensor orientation of Val in *N*-acetylvaline, which has β-sheet torsion angles. The resulting CSA tensor parameters agree very well with the quantum chemical calculations in terms of both the magnitude and the

orientation. This suggests that the predicted Cα tensor orientation difference between various secondary structure motifs may indeed be present. Experiments on the Cα tensor orientations of helical peptides are currently in progress.

The Cα CSA tensor orientation may be useful as an additional tool for protein structure refinement, especially when the CSA magnitudes give ambiguous information on secondary structure. This technique is not restricted to the measurement of Cα tensor orientations but is generally applicable for any organic compounds and functional groups. The amide nitrogen and carbonyl tensors in proteins may also be measured in this way. Further, the CSA modulation sequences presented here can be extended to incorporate a third, isotropic, dimension to enhance site resolution in larger molecules. These dipolar-modulation techniques have high sensitivity: the 2D spectra of the unlabeled methylmalonic acid and NAV were acquired in 2−20 h. Finally, this robust CSA recoupling technique provide a promising means for studying molecular motions in complex systems with site resolution.

**Acknowledgment.** M.H. is a Beckman Young Investigator and the recipient of a NSF CAREER award (MCB-0093398). This research is partially supported by a Research Innovation award from the Research Corporation.

JA017137P